ligands **2-4** that are examined in this study, the hydroxyl groups participate only in anion solvation. Involvement of the anion-binding sites in cation complexation could be a disadvantage if it changes the total number of potential coordination sites for cation binding that might produce conformational changes. Both factors would be expected to influence the selectivity with which different cations are complexed. On the other hand, the separate involvement of the crown ether ring oxygen and hydroxyl group in cation complexation and anion solvation, respectively, observed for the metal salt complexes with crown ether alcohols **2-4** should maintain cation selectivity while enhancing with which the metal salt is transported into an organic medium in solvent extraction or liquid membrane transport processes.

Synthetic attempts are now underway to provide additional crown ether alcohols with structures suitable for simultaneous cation complexation and intracomplex anion solvation.

Acknowledgment. Partial support of this research by the Robert A. Welch Foundation (Grant D-775 to R.A.B.) is gratefully acknowledged. Appreciation is also expressed to the U.S. Department of Energy, Basic Energy Sciences (Grant DE-FG02-13463), and the State of Utah Centers of Excellence Program for partial support of this research.

Supplementary Material Available: Tables 1S-4S, giving atomic positional parameters and thermal parameters for non-hydrogen atoms and alcohol hydrogen atoms, bond lengths and angles for non-hydrogen atoms, anisotropic temperature factors, and calculated coordinates of hydrogen atoms for **2**·LiNCS, Tables 5S-8S, giving atomic positional parameters and thermal parameters for non-hydrogen and alcohol hydrogen atoms, bond lengths and angles for non-hydrogen atoms, anisotropic thermal parameters, and calculated coordinates of hydrogen atoms for **3**·LiNCS, Tables 9S-12S, giving positional parameters and thermal parameters for non-hydrogen atoms, bond lengths and angles for non-hydrogen atoms, anisotropic thermal parameters, and calculated coordinates of hydrogen atoms for **4**·LiNCS, and Tables 13S-16S, giving atomic positional parameters and thermal parameters for non-hydrogen and alcohol hydrogen atoms, bond lengths and angles for non-hydrogen atoms, anisotropic temperature factors, and calculated coordinates for hydrogen atoms for **4**·$LiNO_3$ (18 pages); Tables 17S-20S, giving observed and calculated structure factors for **2**·LiNCS, **3**·LiNCS, **4**·LiNCS, and **4**·$LiNO_3$ (56 pages). Ordering information is given on any current masthead page.

Chemistry of Catalytic Dehydrogenative Oligomerization of Tetrahydroquinoline and Structural Characterization of Nonsubstituted Quinoline Oligomers

L. Y. Chiang,* J. W. Swirczewski, R. Kastrup, C. S. Hsu, and R. B. Upasani

Contribution from Corporate Research Laboratory, Exxon Research and Engineering Company, Annandale, New Jersey 08801. *Received July 24, 1990*

Abstract: A new catalytic dehydrogenative polycondensation (CDHP) of 1,2,3,4-tetrahydroquinoline (THQ) using transition metal sulfides or tris- or bis(*o*-aminobenzenethiolate) complexes of groups VIB, VIIB, and VIII transition metals as catalyst precursors is described. The method provides a direct route to the synthesis of nonsubstituted quinoline oligomers, which have not been prepared by known methods. The effective heterogeneous CDHP catalysts were generated in situ in reaction media from precursors by a preheating treatment at 180-210 °C. These active catalysts were found to consist of metal and sulfur stoichiometric composition approaching MoS_2, ReS_2, RuS, RhS_2, PtS, and PdS. We observed a periodic trend on the CDHP activities of transition metal sulfides, showing a maximum oligomer yield (97%) with a ruthenium sulfide catalyst. The structure of quinoline oligomers was elucidated on the basis of X-ray crystallographic studies and various spectroscopic data including the 2D COSY ^1H NMR spectra. The full structural characterization of two quinoline dimers and a trimer, which were successfully isolated from the bulk product, resolved the puzzle of carbon positions at the ring conjunction between quinoline moieties in oligomers. The first dimer of 2,3'-biquinoline crystallized in a space group of $P2_1/a$ (No. 14) with the monoclinic cell dimensions a = 12.492 (2) Å, b = 5.3821 (9) Å, c = 19.253 (3) Å, and β = 100.20 (1)°, showing a quinoline ring conjunction at carbons C_2 and C_3'. The second dimer of 2,6'-biquinoline crystallized in a space group of Pa (No. 7) with the monoclinic cell dimensions a = 8.1687 (6) Å, b = 5.9748 (5) Å, c = 13.126 (1) Å, and β = 95.032 (7)°, showing a quinoline ring conjunction at carbons C_2 and $C_{6'}$. The structure of one quinoline trimer was found to contain two quinoline ring conjunctions at carbons C_2-$C_{6'}$ and $C_{2'}$-$C_{3''}$. On the basis of results from the structural and kinetic studies, a hypothetical CDHP reaction mechanism was proposed. That leads to two major oligomeric quinoline products **1a** and **1b** differing in only the orientation of the head unit in structure. In the CDHP chemistry, we conclude that a delicate balance between dehydrogenation and polymerization activities of catalyst is required to optimize the yield and the molecular weight of resulting products. We also observed a coexistence of hydrogenation and dehydrogenation activity, probably at different surface sites of transition metal sulfide.

Transition metal sulfides (TMS) have been shown to display the catalytic behavior in both the heterogeneous hydrogenation (in the presence of a low hydrogen pressure) and dehydrogenation (in the absence of hydrogen) of organic compounds in a reversible manner.[1] They have been used extensively in the industrial process as hydrotreating catalysts and the synthetic chemistry to add or remove hydrogen from organic molecules. Under high hydrogen pressure (>1000 psi) transition metal sulfides exhibit hydrodesulfurization (HDS) and hydrodenitrogenation (HDN) activities in addition to hydrogenation. Thus, they are valuable heterogeneous catalysts used for the removal of sulfur and nitrogen from heavy petroleum feedstocks.[2] In both the hydrogenation and

Scheme I

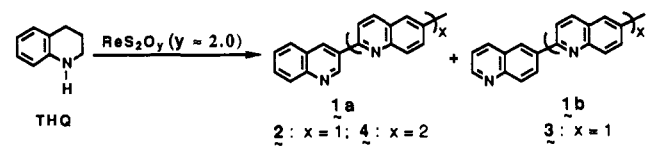

(1) Weiser, O.; Landa, S. *Sulfide Catalysts: Their Properties and Applications*; Pergamon: Oxford, 1973; p 370.

0002-7863/91/1513-6574$02.50/0

dehydrogenation reactions, the process involves the absorption of organic substrates onto catalyst surface, followed by a hydrogen transfer between organic substrates and catalyst surface. The understanding of surface reactivities of TMS is a complex issue. It involves parameters such as the physical and chemical structure of reaction site and several electronic factors on surface including the orbital occupation of the HOMO, the degree of covalency of the metal–sulfur bond, and the metal–sulfur covalent bond strength.[3] The lack of well-defined surface structure and location of reactive sites often hindered the direct mechanistic study of chemical reaction on surface.

Recently, we reported[4,5] the dehydrogenative reactivity of rhenium sulfide on organic heterocyclic molecules such as 1,2,3,4-tetrahydroquinoline (THQ), resulting in an oligomerized product **1** as nonsubstituted quinoline oligomers **1a** and **1b** instead of quinoline as a normal dehydrogenated product as shown in Scheme I. The chemistry represents a new approach to the synthesis of rigid rodlike linear polyaromatic heterocyclics. It serves as a prototype for the preparation of functionalized polyquinolines and polyquinoline related polymers such as polyquinoxalines. The observation can be interpreted by the reversibility of hydrogenation–dehydrogenation reactivities of rhenium sulfides on quinoline analogue molecules. In the absence of hydrogen, transition metal sulfides behave as hydrogen absorbers to convert THQ molecules to dihydroquinolines (DHQ) and then initiate the oligomerization reaction of DHQ. To understand the chemistry of this unique surface dehydrogenative reactivity, we carried out a systematic study through the evaluation and identification of products as well as key reaction intermediates, via kinetic measurements, to elucidate the plausible reaction pathway.

Experimental Section

All NMR spectra were acquired on a Varian XL300 or a Brucker 360 spectrometer in $CDCl_3$ or CD_3CO_2D depending upon the solubility of the oligomer fraction. APT (i.e., attached proton test pulse sequence) spectra were used to assign protonated versus unprotonated carbons on the quinoline dimers. COSY 2D (two dimensional ^1H–^1H correlated spectroscopy) spectra were used to determine ^1H–^1H coupling, and therefore the structure of oligomers. The CPMAS (cross-polarization magic angle spinning) technique was used for the solid-state ^{13}C NMR spectra. A Finnigan TSQ-46B GC/MS/MS tandem quadrupole mass spectrometer was used for the mass spectrometric analysis of quinoline dimers.

Materials Preparation. 1,2,3,4-Tetrahydroquinoline was purchased from Aldrich Chemical Co. and purified by distillation over P_2O_5. The synthesis of heterogeneous high surface area rhenium sulfide (HSRS) catalyst precursors was described previously.[6] Soluble catalyst precursors such as tris(*o*-aminobenzenethiolato)rhenium complexes $Re(abt)_3$ and $Re(abt)_2(C_6H_4NS)$ were prepared from ammonium perrhenate and *o*-aminothiophenol in a solution mixture of H_2SO_4, ethanol, and H_2O according to the reported procedure.[7]

2,3′-Biquinoline (**2**) and 2,6′-biquinoline (**3**) were isolated from the hexane-soluble fraction of quinoline oligomers **1** by thin-layer chromatography (silica gel), using a mixture of $CHCl_3$–EtOAc (4:1) as eluent, corresponding to R_f 0.6 and 0.3, respectively. Crystals of dimers **2** and **3** were recrystallized from ethanol with melting points of 164 and 140 °C, respectively. A mixture of quinoline trimers was isolated from the methylene chloride soluble fraction of oligomers and purified by repeated GPC runs using a combination of five Waters μ-Styragel columns (from high-porosity 10^4- and 10^3-Å columns to low-porosity 500- and 100-Å columns) with tetrahydrofuran as solvent at ambient temperature. The molecular weight calibration is performed based on the oligomeric styrene standards. From this trimer mixtures, 2,6′:2′,3″-triquinoline (**4**) was obtained through the thin-layer chromatography (silica gel, R_f 0.5) using chloroform as eluent.

Preparation of Ruthenium Sulfide Catalyst Precursors. A three-neck round-bottom flask (500 mL) equipped with a condenser and an inert gas bubbler was charged with lithium sulfide (7.2 g, 0.12 mol) and absolute ethanol (350 mL). To the solution was added ammonium hexachlororuthenate(IV) (21 g, 0.06 mol) portionwise over a period of 1 h. The mixture was stirred at 40 °C under N_2 for overnight to afford a black suspension. The insolubles in suspension were filtered, washed repeatedly with ethanol, and dried to give black solids of ruthenium sulfides (20.5 g). Elemental analysis of the dried product best fits a composition of $(NH_4)_{1.3}Li_{0.5}RuS_{1.5}Cl_{1.7}$.

Dehydrogenative Oligomerization of THQ with Ruthenium Sulfide Precursor. A single-neck round-bottom flask equipped with a condenser and an inert gas bubbler was charged with a solution of 1,2,3,4-tetrahydroquinoline (200 g, 1.54 mol), which was thoroughly mixed with a 3% by weight of ruthenium sulfides (6 g) prepared from the method described above. The suspended mixture was maintained under an argon at atmospheric pressure and heated at 210 °C for 4 h and then at 270 °C for 24 h. At this temperature, a gentle reflux of tetrahydroquinoline was obtained. At the end of reaction, the resulting products were cooled to room temperature to give a dark solid. It was transferred into a solution mixture of diethyl ether–hexane (1:5) (1 L), forming a suspension, which was stirred overnight at room temperature. The insoluble solid was then filtered and washed with an another portion of diethyl ether–hexane (1:5) (300 mL). A repeated methylene chloride extraction of the solid separated the product into a methylene chloride soluble fraction and a methylene chloride insoluble fraction. After evaporation of solvent, the orange-brown solid from the methylene chloride soluble fraction was washed with cool methanol (500 mL) to give brownish yellow solids of quinoline oligomer (QO, **1**; x = 2–12) in 41% yield (82 g). The methanol washings contained partially hydrogenated quinoline oligomer (HQO) as orange-red semisolids in 3% yield (6.0 g). The methylene chloride insoluble fraction were subsequently treated with concentrated HCl and stirred overnight. The resulting acid solution was filtered through a sintered glass frit under vacuum and then neutralized by NaOH to effect the precipitation of a gray solid of the higher molecular weight quinoline oligomers (QO, **1**; $x > 10$) in 53% yield (106 g).

Dehydrogenative Oligomerization of THQ with $Re(abt)_3$ Precursor. Tris(*o*-aminobenzenethiolato)rhenium $Re(abt)_3$ or $Re(abt)_2(C_6H_4NS)$ (3.3 g), which is equivalent to 3% by weight of ReS_2, was dissolved in 1,2,3,4-tetrahydroquinoline (50 mL). The mixture was allowed to react at 210 °C for 4 h and then at 270 °C for 5 days under 1 atm of nitrogen. After being cooled to room temperature, the reaction mixture was transferred into a solution mixture of diethyl ether–hexane (1:5) (500 mL). The resulting suspension was stirred overnight at room temperature. The insoluble solid was filtered and washed with an another portion of diethyl ether–hexane (1:5) (140 mL). The mother liquor was found to contain a 8% yield (4 g) of quinoline. A similar procedure as described above was used to separate the insoluble solids into fractions of product as follows: the methylene chloride soluble fraction of quinoline oligomers (QO, **1**; x = 2–12) in 57% yield (28.6 g), the partially hydrogenated quinoline oligomers (HQO) in 23% yield (11.3 g), and the methylene chloride insoluble fraction of quinoline oligomers (QO, **1**; $x > 11$) in 5% yield (2.5 g). Finally, no 1,2,3,4-tetrahydroquinoline was recovered in the product.

X-ray Crystal Structure Determination of Quinoline Dimers. All measurements were made on a Rigaku AFC6R diffractometer with graphite-monochromated Cu Kα radiation and a 12-KW rotating anode generator. The data were collected at 23 ± 1 °C by the ω–2θ scan technique to a maximum 2θ value of 118.1°. Azimuthal scans of several reflections indicated no need for an absorption correction. The data were corrected for Lorentz and polarization effects.

2,3′-Biquinoline (2). A clear plate crystal having approximate dimensions of 0.05 × 0.15 × 0.15 mm mounted on a glass fiber was used for the measurement. Due to a paucity of observed data, none of the atoms could be refined anisotropically. The stereochemistry of the compound was derived from the values of isotropic thermal parameters of a model in which all of the atoms were assigned as carbon. Two atoms were assigned as nitrogen in the final model had significant lower thermal parameters, when assigned as carbon, than did any of the other atoms. When these two atoms were reassigned as nitrogen, the residual values for the model showed a marked improvement. Cell constants and an orientation matrix for the data collection, obtained from the least-squares refinement using the angles of 25 reflections in the range $44.2 < \theta < 89.3°$, corresponded to a monoclinic cell with dimensions a = 12.492 (2) Å, b = 5.3821 (9) Å, c = 19.253 (3) Å, and β = 100.20 (1)°. Crystallographic details are presented in Table I. Systematic absences and the subsequent least-squares refinement determined the space group to be $P2_1/a$ (No. 14), with an asymmetric unit consisting of one molecule in a general position of the unit cell. The model of molecular packing

(2) Pecoraro, T. A.; Chianelli, R. *J. Catal.* **1981**, *67*, 430.
(3) Harris, S.; Chianelli, R. *J. Catal.* **1984**, *86*, 400.
(4) Chiang, L. Y.; Chianelli, R. R. *J. Chem. Soc., Chem. Commun.* **1986**, 1461. Chiang, L. Y.; Chianelli, R. R. U.S. Patent 4,727,135, Feb 23, 1988.
(5) Chiang, L. Y.; Swirczewski, J. W.; Chianelli, R. R.; Stiefel, E. I. *Catal. Lett.* **1988**, *1*, 177; Chiang, L. Y.; Swirczewski, J. W.; Chianelli, R. R. *Polym. Prepr. (Am. Chem. Soc. Div. Polym. Chem.)* **1988**, *29*, 210.
(6) Chiang, L. Y.; Swirczewski, J. W.; Passaretti, J. D.; Chianelli, R. R. *Solid State Ionics* **1989**, *32/33*, 988.
(7) Gardner, J. K.; Pariyadath, N.; Corbin, J. L.; Stiefel, E. I. *Inorg. Chem.* **1978**, *17*, 897.

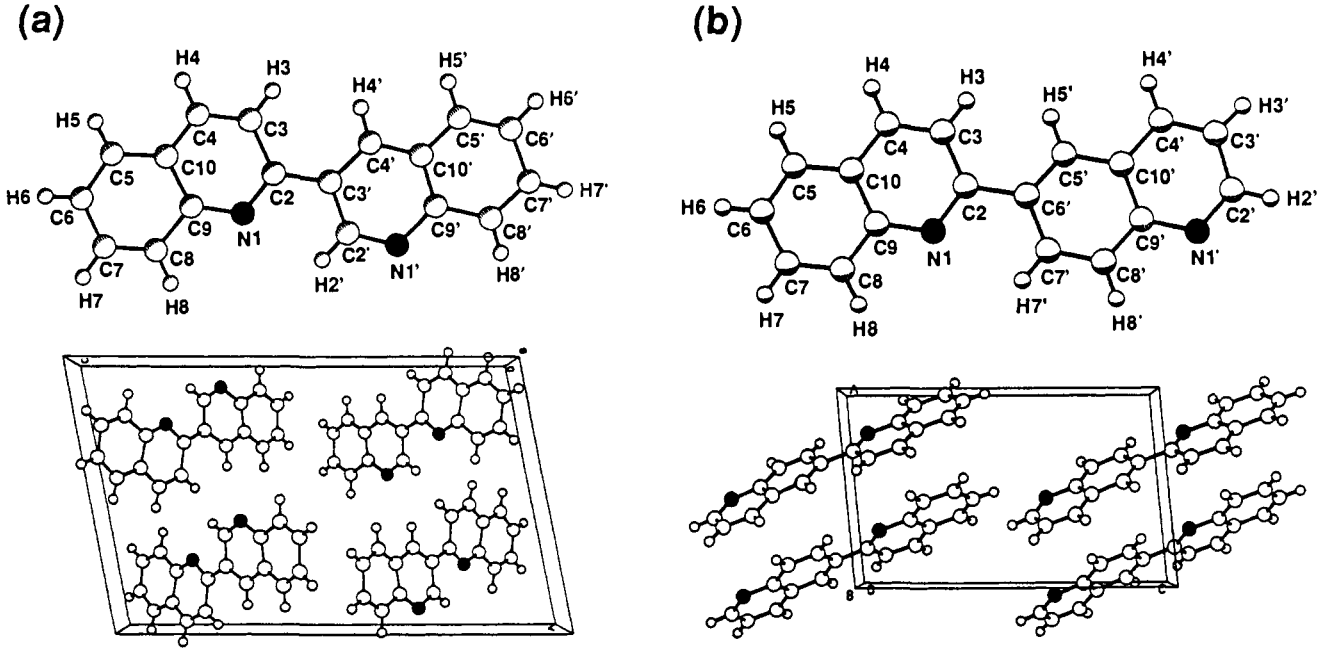

Figure 1. Atom labeling and the model of monoclinic molecular packing for (a) 2,3'-biquinoline (**2**, projected down the *b* axis) and (b) 2,6'-biquinoline (**3**, projected down the *b* axis).

Table I. Crystallographic Parameters for 2,6'-Biquinoline and 2,3'-Biquinoline

	2,6'-biquinoline	2,3'-biquinoline
formula	$C_{18}H_{12}N_2$	$C_{18}H_{12}N_2$
formula weight	256.31	256.31
crystal system	monoclinic	monoclinic
space group	*Pa* (No. 7)	$P2_1/a$ (No. 14)
a (Å)	8.1687 (6)	12.492 (2)
b (Å)	5.9748 (5)	5.3821 (9)
c (Å)	13.126 (1)	19.253 (3)
β (deg)	95.032 (7)	100.20 (1)
V (Å^3)	638.2 (2)	1273.9 (3)
Z	2	4
D_{calc} (g/cm^3)	1.32	1.34
crystal dimens (mm)	0.25 × 0.18 × 0.30	0.05 × 0.15 × 0.15
F_{000}	264	536
temp (°C)	23	23
radiation	Cu Kα (λ = 1.54178 Å)	Cu Kα (λ = 1.54178 Å)
abs. coeff (cm^{-1})	6.29	6.31
scan type	ω–2θ	ω–2θ
$2\theta_{max}$ (deg)	118.1	118.2
function minimized	$\sum w(\|F_o\| - \|F_c\|)^2$	$\sum w(\|F_o\| - \|F_c\|)^2$
least-square weights	$4F_o^2/\sigma^2(F_o^2)$	$4F_o^2/\sigma^2(F_o^2)$
total no. reflcns measd	1082	2161
unique no. reflcns	1068 (R_{int} = 0.003)	2057 (R_{int} = 0.05)
no. observns	854 ($I > 3.0\sigma(I)$)	407 ($I > 2.58\sigma(I)$)
no. variables	180	82
residuals: R_u; R_w	0.036; 0.051	0.099; 0.111
max peak in final diff map (e/Å^3)	0.13	0.33
max peak in final diff map (e/Å^3)	−0.13	−0.40

and the atom labeling for 2,3'-biquinoline can be found in Figure 1a. The tables of intramolecular bond distances, intramolecular bond angles, positional coordinates, the general displacement parameter expression, torsion or conformation angles, intermolecular distances, and least-squares planes for **2** are provided as supplementary material (Tables S1–S7). The structure factor amplitude tables for $C_{18}H_{12}N_2$ (**2**) are also available as supplementary material (Table S15). The torsional angles of both N1–C2–C3'–C2' and N1–C2–C3'–C4' were found to be 2°, indicating a high degree of coplanarity between two quinoline moieties at ring conjunction. The chemical structure of compound **2** is also confirmed by the 2D homonuclear correlated ^{1}H NMR and ^{13}C NMR APT spectroscopic studies discussed below.

2,6'-Biquinoline (3). A pale yellow parallel crystal having approximate dimensions of 0.25 × 0.18 × 0.30 mm was used. Cell constants and an orientation matrix for the data collection, obtained from least-squares refinement using the angles of 25 reflections in the range $106.0 < 2\theta < 117.8°$, corresponded to a monoclinic cell with dimensions *a* = 8.1687 (6) Å, *b* = 5.9748 (5) Å, *c* = 13.126 (1) Å, and β = 95.032 (7)°. Crystallographic details for compound **3** are presented in Table I. Systematic absences and the subsequent least-squares refinement determined the space group to be *Pa* (No. 7) with two molecules per unit cell. The model of molecular packing and the atom labeling for 2,6'-biquinoline can be found in Figure 1b. Tables of intramolecular bond distances, intramolecular bond angles, positional coordinates, anisotropic thermal parameters, torsion or conformation angles, intermolecular distances, and least-squares planes for compound **3** are provided as supplementary material (Tables S8–S14). The structure factor amplitude tables for $C_{18}H_{12}N_2$ (**3**) are also available as supplementary material (Table S16). The torsional angles of N1–C2–C6'–C5' and N1–C2–C6'–C7' were found to be 1.2° and 0.4°, respectively, indicating a high degree of coplanarity between quinoline moieties at ring conjunction similar to that of 2,3'-biquinoline.

Table II. Chemical Shift (ppm) of Protons in 2,3'-Biquinoline and 2,6'-Biquinoline

	2,3'-biquinoline	2,6'-biquinoline
H3	8.31 (d, *J* = 8.7 Hz)	8.27 (d, *J* = 8.6 Hz)
H4	8.03 (d, *J* = 8.7 Hz)	8.02 (d, *J* = 8.6 Hz)
H5	8.00 (dd, *J* = 8.4, 1.3 Hz)	7.85 (dd, *J* = 7.5, 1.5 Hz)
H6	7.62 (ddd, *J* = 8.4, 7.9, 1.3 Hz)	7.55 (ddd, *J* = 7.5, 7.5, 1.2 Hz)
H7	7.79 (ddd, *J* = 7.9, 8.5, 1.3 Hz)	7.76 (ddd, *J* = 7.5, 7.7, 1.5 Hz)
H8	8.24 (dd, *J* = 8.5, 1.3 Hz)	8.22 (dd, *J* = 7.7, 1.2 Hz)
H2'	9.77 (d, *J* = 1.7 Hz)	8.96 (d, *J* = 4.3 Hz)
H3'		7.45 (dd, *J* = 4.3, 8.3 Hz)
H4'	8.95 (d, *J* = 1.7 Hz)	8.30 (d, *J* = 8.3 Hz)
H5'	7.87 (dd, *J* = 8.4, 1.5 Hz)	8.62 (s)
H6'	7.59 (ddd, *J* = 8.4, 7.4, 1.5 Hz)	
H7'	7.78 (ddd, *J* = 7.4, 7.6, 1.5 Hz)	8.60 (d, *J* = 8.7 Hz)
H8'	8.23 (dd, *J* = 7.6, 1.5 Hz)	8.27 (d, *J* = 8.7 Hz)

NMR Spectroscopic Structural Studies. Determination of the structure of dimers was aided by the use of 2D homonuclear correlated ^{1}H NMR and ^{13}C NMR APT spectra. Complete assignments of protons were made on the basis of the 2D COSY experiment and the proton coupling constants. The APT experiment[8-10] is a spin echo pulse sequence that allows the observed spins to evolve differently as a function of the number of attached hydrogen. The spectra are able to discriminate carbons having one versus zero attached hydrogen. With the pulse interval chosen for the spectra shown in Figure 3, the spins evolved such

(8) Rabenstein, D. L.; Nakashimi, T. T. *Anal. Chem.* **1979**, *51*, 1465A.
(9) LeCocq, C.; Lallemond, J. Y. *J. Chem. Soc., Chem. Commun.* **1981**, 150.
(10) Patt, S. L.; Shoolery, J. N. *J. Magn. Reson.* **1982**, *46*, 535.

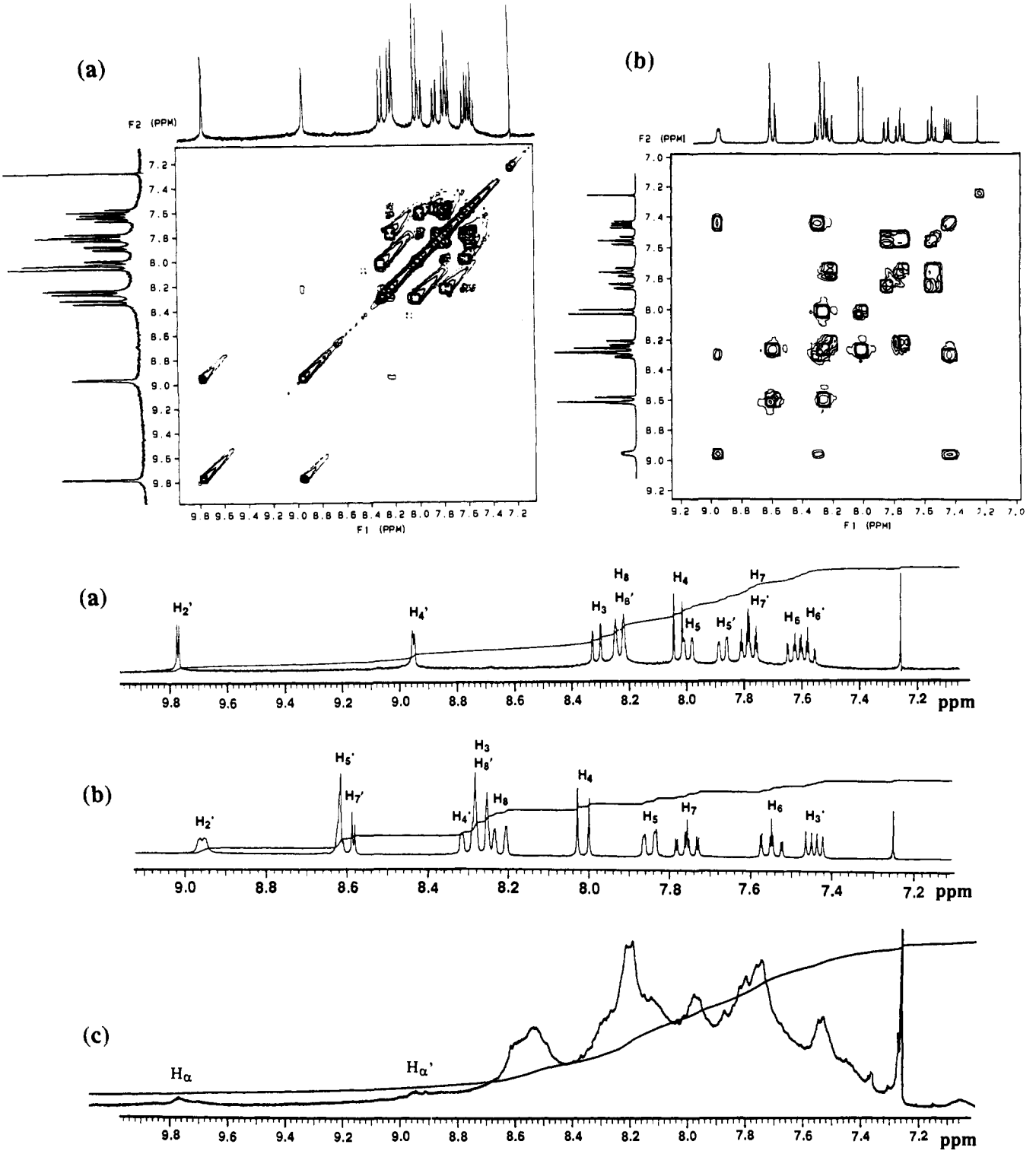

Figure 2. 300-MHz 2D homonuclear-corrected ^1H NMR spectra (COSY) of (a) 2,3'-biquinoline in $CDCl_3$ and (b) 2,6'-biquinoline in $CDCl_3$ and (c) ^1H NMR spectrum of the methylene chloride insoluble and acetic acid soluble fraction of oligomers.

that carbon nuclei having one bound hydrogen have peaks pointing downward and carbon nuclei having no bound hydrogen have peaks pointing upward.

2,3'-Biquinoline. The assignment of protons in 2,3'-biquinoline based on the 2D COSY spectrum is shown in Figure 2a and summarized in Table II. We found that the protons $H_{2'}$ (α proton) and $H_{4'}$ have downfield chemical shifts of 9.77 and 8.95 ppm, respectively. The coupling constants $J_{H_3\text{-}H_4}$, $J_{H_5\text{-}H_6}$, $J_{H_6\text{-}H_7}$, $J_{H_7\text{-}H_8}$, $J_{H_{5'}\text{-}H_{6'}}$, $J_{H_{6'}\text{-}H_{7'}}$, and $J_{H_{7'}\text{-}H_{8'}}$ were found to be 8.7, 8.4, 7.9, 8.5, 8.4, 7.4, and 7.6 ± 1.0 Hz, respectively. The long-range coupling constants $J_{H_6\text{-}H_8}$, $J_{H_5\text{-}H_7}$, $J_{H_{2'}\text{-}H_{4'}}$, $J_{H_{6'}\text{-}H_{8'}}$, and $J_{H_{5'}\text{-}H_{7'}}$ were measured to be 1.3, 1.3, 1.7, 1.5, and 1.5 ± 0.3 Hz, respectively.

In the ^{13}C NMR APT spectrum of 2,3'-biquinoline (Figure 3a), a total of 18 peaks was observed for the 18 carbons in the dimer, indicating that there are no chemically equivalent carbons. It shows six nonprotonated carbons (upward peaks): four from ring junction carbons (C_9, $C_{9'}$, C_{10}, $C_{10'}$) at 148.2, 148.1, 127.6, and 127.2 ppm and two from carbons C_2 and $C_{3'}$ at 154.4 and 131.9 ppm, respectively, consistent with the structural assignment for quinoline conjunction at C_2 and $C_{3'}$ carbons. By utilizing the reported ^{13}C NMR data for quinoline as a reference,[11] we assigned protonated peaks (downward peaks) at 118.5, 134.3, 137.0, and 149.6 ppm for carbons C_3, $C_{4'}$, C_4, and $C_{2'}$, respectively. The downfield shift (2.7 ppm) of the $C_{4'}$ peak from the C_4 peak is due its carbon position adjacent to the ring conjunction. The rest of the eight protonated peaks

(11) Kidric, J.; Hadzi, D.; Kocjan, D. *Org. Magn. Resonance* **1981**, *15*, 280.

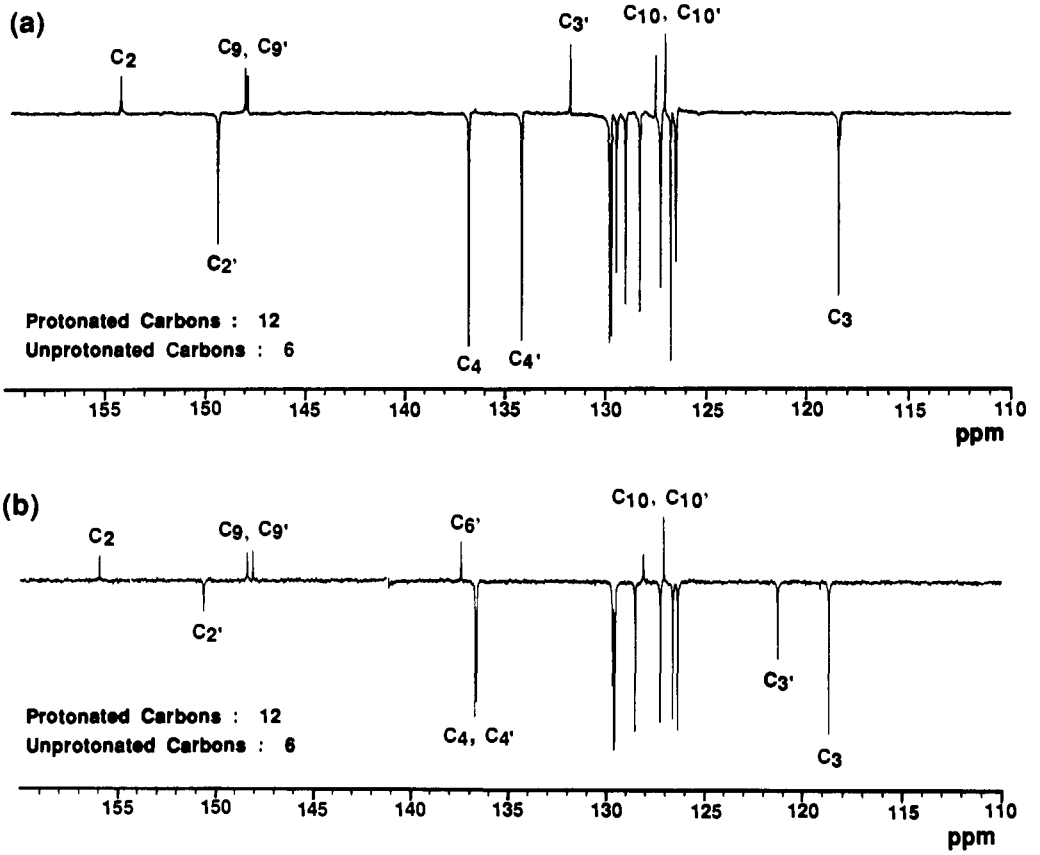

Figure 3. 300-MHz ^{13}C NMR APT (attached proton test pulse sequence) spectra of (a) 2,3'-biquinoline and (b) 2,6'-biquinoline in $CDCl_3$.

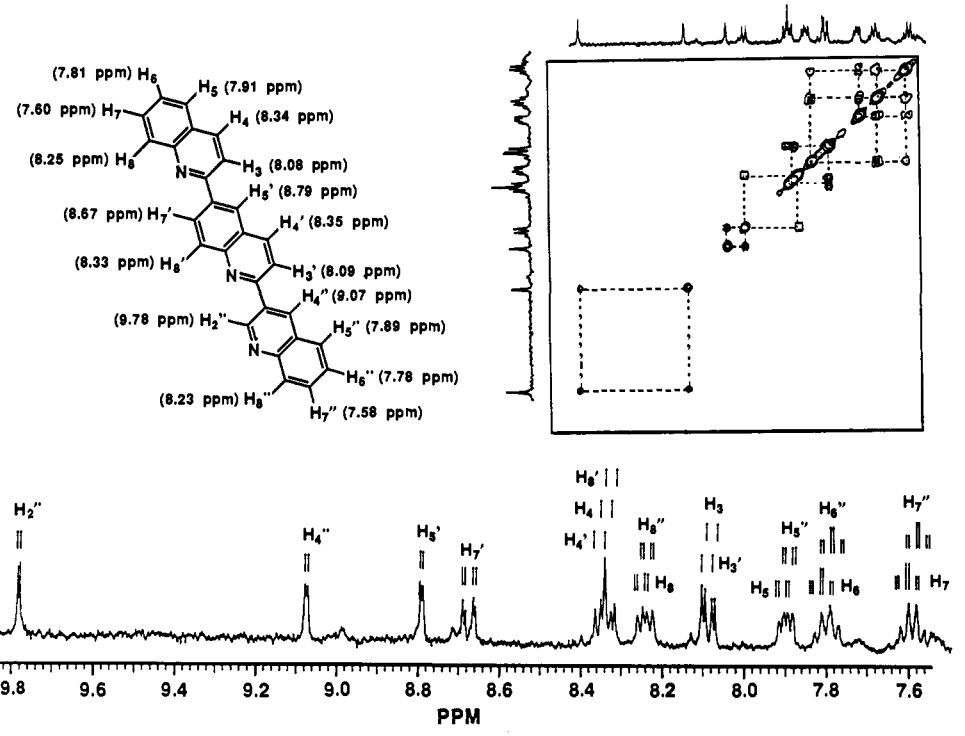

Figure 4. 360-MHz 2D homonuclear-correlated ^1H NMR spectra (COSY) of 2,6':2',3"-triquinoline.

between 126 and 131 ppm for carbons C_5, C_6, C_7, C_8, $C_{5'}$, $C_{6'}$, $C_{7'}$, and $C_{8'}$ remain unresolved.

2,6'-Biquinoline. The assignment of protons in 2,6'-biquinoline based on the 2D COSY spectrum as shown in Figure 2b is summarized in Table II. We found that the protons of $H_{2'}$ (α proton), $H_{5'}$, and $H_{7'}$ have downfield chemical shifts of 8.96, 8.62, and 8.60 ppm, respectively. The coupling constants $J_{H_3\text{-}H_4}$, $J_{H_5\text{-}H_6}$, $J_{H_6\text{-}H_7}$, $J_{H_7\text{-}H_8}$, $J_{H_2'\text{-}H_3'}$, $J_{H_3'\text{-}H_4'}$, and $J_{H_7'\text{-}H_8'}$ equal 8.6, 7.5, 7.5, 7.7, 4.3, 8.3, and 8.7 ± 1.0 Hz, respectively. The long-range coupling constants $J_{H_5\text{-}H_7}$ and $J_{H_6\text{-}H_8}$ were measured to be 1.5 and 1.2 ± 0.5 Hz, respectively.

In the ^{13}C NMR APT spectrum of 2,6'-biquinoline (Figure 3b), there are 18 peaks observed for 18 carbons in the dimer, indicating no chemically equivalent carbons present in the molecule. It shows six nonprotonated carbons (upward peaks): four from ring junction carbons (C_9, $C_{9'}$, C_{10}, $C_{10'}$) at 148.4, 148.1, 128.1, and 127.0 ppm and two from carbons C_2 and $C_{6'}$ at 155.9 and 137.4 ppm, respectively. We assigned protonated peaks (downward peaks) at 118.7, 121.3, 136.7, 136.7, and 150.6 ppm to carbons C_3, $C_{3'}$, $C_{4'}$, C_4, and $C_{2'}$, respectively. The rest of

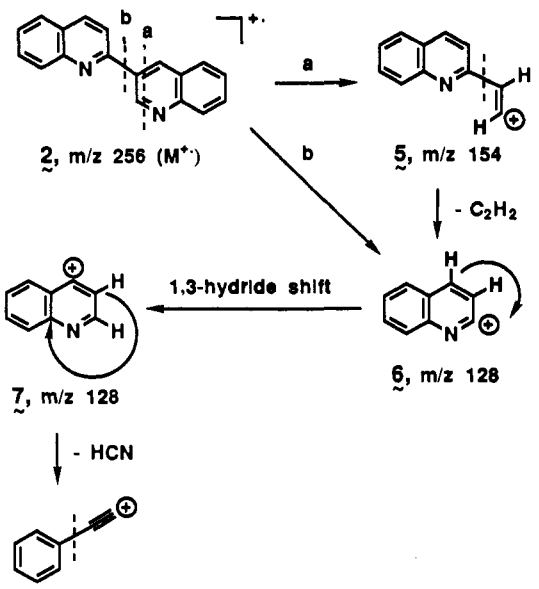

Figure 5. Fragmentation pathway of 2,3'-biquinoline via the formation of the m/z 154 ion.

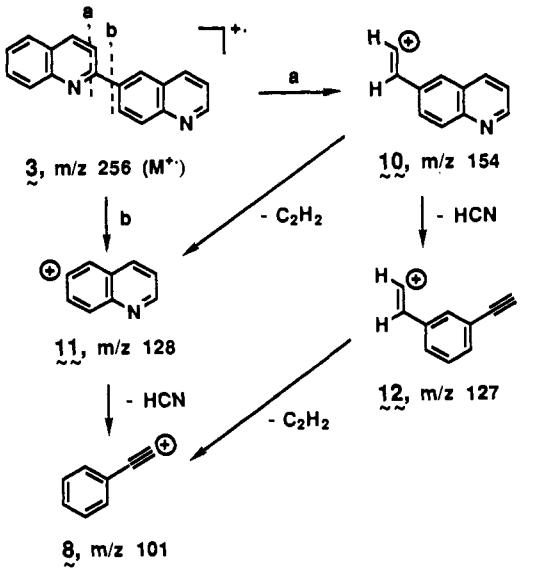

Figure 6. Fragmentation pathway of 2,6'-biquinoline via the formation of the m/z 154 ion.

the seven protonated peaks between 126 and 130 ppm for carbons C_5, C_6, C_7, C_8, $C_{5'}$, $C_{7'}$, and $C_{8'}$ remain unresolved.

2,6':2',3''-Triquinoline. The assignment of protons in 2,6':2',3''-triquinoline based on the 2D COSY spectrum as shown in Figure 4 is summarized as follows: δ 7.58 (ddd, $H_{7''}$), 7.60 (ddd, H_7), 7.78 (ddd, $H_{6''}$), 7.81 (ddd, H_6), 7.89 (dd, $H_{5''}$), 7.91 (dd, H_5), 8.08 (d, H_3), 8.09 (d, $H_{3'}$), 8.23 (dd, $H_{8''}$), 8.25 (dd, H_8), 8.33 (dd, $H_{8'}$), 8.34 (dd, H_4), 8.35 (dd, $H_{4'}$), 8.67 (dd, $H_{7'}$), 8.79 (d, $H_{5'}$), 9.07 (d, $H_{4''}$), 9.78 (d, $H_{2''}$). Protons of $H_{2''}$ (α proton), $H_{4''}$, $H_{5'}$, and $H_{7'}$ have downfield chemical shifts between 8.6 and 9.8 ppm. The coupling constants $J_{H_3\text{-}H_4}$, $J_{H_5\text{-}H_6}$, $J_{H_6\text{-}H_7}$, $J_{H_7\text{-}H_8}$, $J_{H_{3'}\text{-}H_{4'}}$, $J_{H_{7'}\text{-}H_{8'}}$, $J_{H_{5''}\text{-}H_{6''}}$, $J_{H_{6''}\text{-}H_{7''}}$, and $J_{H_{7''}\text{-}H_{8''}}$ were found to be 8.6, 8.3, 8.3, 8.6, 8.6, 9.0, 8.6, 8.3, and 8.6 ± 1.0 Hz, respectively. The long-range coupling constants $J_{H_5\text{-}H_7}$, $J_{H_6\text{-}H_8}$, $J_{H_{5'}\text{-}H_{7'}}$, $J_{H_{2''}\text{-}H_{4''}}$, $J_{H_{5''}\text{-}H_{7''}}$, and $J_{H_{6''}\text{-}H_{8''}}$ are measured to be 1.7, 1.7, 2.0, 2.0, 1.7, and 1.7 ± 0.5 Hz, respectively.

Mass Spectrometric Studies of Quinoline Dimers and Trimer. In a single-stage mass spectrometric operation using a triple-stage quadrupole instrument, either the first quadrupole (Q1) or the third quadrupole (Q3) was used as a mass analyzer, while the other one allowed all the ions to pass through. In a double-stage mass spectrometric (MS/MS) operation, parent, daughter, and neutral loss experiments can be performed.[12,13] Here, only the results from daughter experiments are reported. The daughter spectra of the selected ions were acquired by tuning the selected mass at the Q1 and scanning the Q3 for its daughter (fragment) ions. In all modes, the second quadrupole (Q2) allowed all the ions to pass through and functioned as a collimation or focusing device during collision induced dissociation in the MS/MS experiments.

The difference between single-stage mass spectra of isomers **2** and **3** are significant and make it possible to distinguish between 2,3'-biquinoline and 2,6'-biquinoline. Specific structural information can be obtained by the use of daughter spectra of the selected ions. The 70-eV EI single-stage mass spectra of 2,3'-biquinoline and 2,6'-biquinoline are available as supplementary material (Figure S1a,b). In both figures, abundant molecular ions were present, which confirm the molecular weight of quinoline dimers at 256. The most significant fragment ion is at m/z 128 resulting from carbon–carbon bond cleavage at the ring conjunction between the two quinoline units. The fragmentation patterns of **2** and **3** are similar except for the more abundant m/z 154 ion being present in the spectrum of 2,3'-biquinoline. A similar difference was observed in the daughter spectra of the molecular ions of these two isomers.

The daughter spectra of the m/z 154 ions, which are available as supplementary material (Figure S1c,d), for 2,3'-biquinoline and 2,6'-biquinoline were used to differentiate the structure of quinoline dimers with a different displacement of nitrogen atoms in the heterocyclic ring. Figures 5 and 6 summarize the proposed fragmentation pathways via the formation of the m/z 154 ions. The most significant loss found in the m/z 154 daughter spectrum of 2,3'-biquinoline is a loss of acetylene (C_2H_2) forming the m/z 128 ion (**5** → **6**), while that of 2,6'-biquinoline is a loss of HCN forming the m/z 127 ion (**10** → **12**), because the loss of HCN in the m/z 154 ion is easier in 2,6'-biquinoline, which has no substitution on $C_{2'}$, than 2,3'-biquinoline. The HCN loss, however, becomes significant for the latter after losing acetylene (**6** → **7** → **8**).

The mass spectrum (EI) of 2,6':2',3''-triquinoline (supplementary material (Figure S1e)) shows the molecular ion M^+ at m/z 383. The simple bond cleavages at the ring conjunctions yield fragment ions at m/z 128 and 255, containing one and two quinoline units, respectively. Consecutive fragmentations of these ions yield the fragment ions of m/z 154 and 101 similar to those discussed above.

Results and Discussion

It is known that polyquinoline derivatives can be prepared by the Pfitzinger reaction,[14] an electrochemical polymerization,[15] or the Friedlander synthesis.[16] The last method is most widely used and is a base-catalyzed reaction between 2-aminobenzaldehyde and acetaldehyde. Utilization of the Friedlander reaction in the synthesis of polyquinoline derivatives has been reviewed.[17] However, the method was reported to be most suitable for the preparation of substituted polyquinolines but is problematic in a similar preparation of nonsubstituted polyquinoline.[18] This is mainly due to the side reaction of the aldehyde functionality if an ortho amino aldehyde is used instead of ortho amino ketone in the Friedlander reaction. The described rhenium sulfide chemistry overcomes these difficulties and provides a potential alternative route for the synthesis of nonsubstituted polyquinoline as well as functionalized polyquinolines.

Rhenium sulfide precursors used in this study were prepared by various methods including modified literature procedures.[19-21] As expected, the variation of reaction conditions and reagents resulted in rhenium sulfides with a different chemical composition, crystallinity, and surface area. That, in term, influenced the efficiency of the CDHP reaction in a wide range. Two types of

(12) Yost, R. A.; Enke, C. G. *Anal. Chem.* **1979**, *51*, 1251A.
(13) Slayback, J. R. B.; Story, M. S. *Ind. Res. Dev.* **1981**, 40.
(14) Shopov, I. *Vysokomol. Soedin. Ser., B* **1969**, *11*, 248.
(15) Pham, M. C.; Dubois, J. E.; Lacaze, P. C. *J. Electrochem. Soc.* **1983**, *130*, 346.
(16) Friedlander, P. *Berichte* **1882**, *15*, 2572.
(17) For a review: Stille, J. K. *Macromolecules* **1981**, *14*, 870.
(18) Imai, Y.; Johnson, E. F.; Katto, T.; Kurihara, M.; Stille, J. K. *J. Polym. Sci., Polym. Chem. Ed.* **1975**, *13*, 2233.
(19) Chianelli, R. R.; Dines, M. B. *Inorg. Chem.* **1978**, *17*, 2758.
(20) Traore, K.; Coeffier, G.; Brenet, J. P. *Bull. Soc. Chim. Fr.* **1962**, 361. Ermolaev, M. I.; Basitova, S. M.; Shatkovskaya, N. A. *Izv. Akad. Nauk Tadzh. SSR, Otd. Fiz.-Mat. Geol.-Khim. Nauk* **1979**, *2*, 52. Satpaeva, T. A.; Isakova, R. A.; Polyakova, T. P. *Tr. Inst. Geol. Nauk, Akad. Nauk Kes. SSR* **1963**, *7*, 318.
(21) Wildervanck, J. C.; Jellinek, F. *J. Less Common Metals* **1971**, *24*, 73.

reaction conditions were developed for the synthesis of heterogeneous rhenium sulfide precursors: first, the reaction of ammonium perrhenate with gaseous hydrogen sulfide in an acidic solution and, second, the reaction of ammonium perrhenate or rhenium(V) chloride with nucleophilic sulfide anion. As a result, a rhenium sulfide precursor HSRS with a high surface area (24–45 m^2/g) and a rhenium vs sulfur ratio close to Re_2S_7 gave the best CDHP oligomerization results with 98% yield of QO and HQO oligomers combined, where QO is quinoline oligomers and HQO is the partially hydrogenated quinoline oligomers. This catalyst precursor was prepared by treating ammonium perrhenate in an aqueous acetic acid solution with H_2S at pH 4.2.[6] When the pH value deviated much from 4.2, the reaction resulted in rhenium sulfides with a low surface area of 0.1–2 m^2/g. Nevertheless, the chemical composition of low surface area rhenium sulfides bears a close resemblance to that of the high surface area analogue. Furthermore, we found that 2–4% by weight is the optimum amount of poorly crystalline heterogeneous catalyst precursor required to complete the reaction. Upon decrease of catalyst precursor concentration, both the yield and the average degree of aromaticity of product decline. For example, at a concentration of 0.4% by weight of active catalyst, only 10% yield of soluble oligomers was obtained.

An alternative route to curtail the complexity of rhenium sulfide chemistry discussed above and to improve the consistency of the chemical composition, crystallinity, and surface area of the catalyst is to use the homogeneous catalyst precursor to generate CDHP catalysts in situ in the monomer solution at an elevated temperature. Several molecular rhenium–sulfur complexes have been investigated for this purpose. As a result, tris(*o*-aminobenzenethiolato)rhenium complexes[7] $Re(abt)_3$ (**13a**) and $Re(abt)_2(C_6H_4NS)$ (**13b**) were found to be the most promising reagents

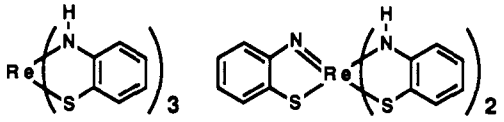

13a **13b**

for the CDHP reaction. All the others gave predominantly a various degree of dehydrogenation with low polymerization activities. Thus, the soluble rhenium complex **13a** or **13b** was converted in situ in THQ to a finely divided active rhenium sulfide catalyst, which produced a high yield of quinoline oligomers (85%) and quinoline (8%). The results indicated that active rhenium sulfides generated from tris(*o*-aminobenzenethiolato)rhenium have a slightly higher overall dehydrogenation activity than that of high surface area rhenium sulfide solids.

We observed a systematic transformation of the rhenium/sulfur composition of catalyst precursors during the early stage of reaction below 210 °C. The chemical reactivity of the transformed intermediates showed a strong correlation to the composition changes. Therefore, it is important to investigate the thermal chemistry of rhenium sulfides for better understanding of their structural evolution upon the heat treatment. According to the thermogravimetric analysis (TGA) diagram, the high surface area rhenium sulfide precursor HSRS can be thermally converted to Re_2S_7 below 200 °C by a removal of weakly held H_2O and an excess of sulfur. Between 200 and 400 °C, Re_2S_7 decomposes to ReS_3 and then to Re_2S_5 at temperatures slightly higher than 400 °C.[20,21] The sulfur to rhenium ratio was found to be 2.43 at 400 °C and 2.22 at 600 °C.[6] Furthermore, it will not be completely converted to ReS_2 until the temperature reaches above 800 °C. We found that, in the presence of 1,2,3,4-tetrahydroquinoline at temperatures between 180 and 210 °C, precursor HSRS was reacted and converted to a suspension of hydrocarbon containing rhenium sulfides with a sulfur to rhenium ratio consistent with a chemical composition of $ReS_{1.9-2.1}O_x$. These thermally treated sulfides are believed to be the actual active catalysts for the CDHP reaction.

In the case of tris(*o*-aminobenzenethiolato)rhenium complexes, the TGA measurement clearly indicated a weight loss starting

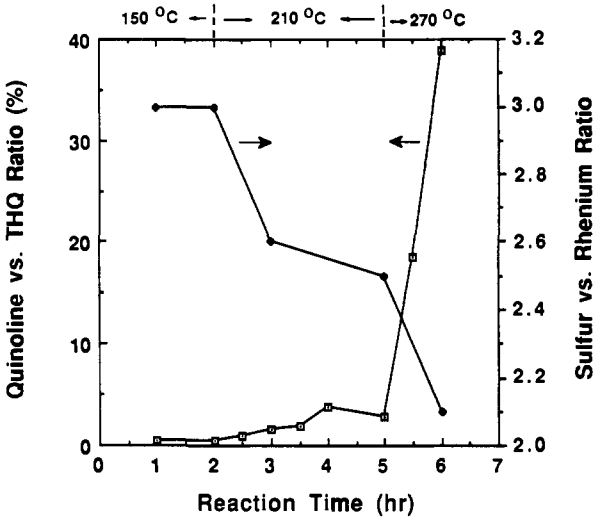

Figure 7. Temperature- and time-dependent thermal conversion of $Re(abt)_3$ to rhenium sulfide solids and their dehydrogenation reactivities.

at 225 °C with derivative maxima at 250, 292, and 350 °C. A 20% weight loss was reached at 500 °C. From these data the change in chemical composition is not obvious. However, similar to the conversion mechanism in the thermal chemistry of rhenium sulfide solids described above, in the presence of THQ molecules both soluble $Re(abt)_3$ and $Re(abt)_2(C_6H_4NS)$ were readily converted to a fine suspension of hydrocarbon-containing rhenium sulfide particles upon a thermal treatment. Figure 7 shows the correlation between thermal transformations of $Re(abt)_3$ and the evolution of their dehydrogenation reactivity. In Figure 7, a sharp loss of aminobenzene and sulfur from $Re(abt)_3$ was indicated in the early stage of reaction with a weight loss of 26.9% within 1 h at 210 °C. Elemental analysis revealed the formulation composition of these rhenium sulfide particles as $ReS_{2.6}C_{7.6}N_{1.1}H_{8.1}O_{1.3}$. The composition stays relatively constant as $ReS_{2.5}C_{7.3}N_{1.1}H_{8.0}O_{1.7}$ in the later stage at this temperature. The infrared spectrum of these thermal intermediates showed a slow development of absorptions at 1119, 900, 438, and 619 cm^{-1} upon the increase of temperature and the reaction time. The former three bands correspond to $-SO_2-$, Re–O, and Re–S absorptions. Evidently, rhenium sulfide polymers are highly reactive to a trace amount of oxygen in the medium. However, the nature of the corresponding structural changes are not clear. When the temperature was raised to 270 °C, the carbon to rhenium and sulfur to rhenium ratios were decreased further to 5.5 and 2.1, respectively, with a 33.3% weight loss from $Re(abt)_3$. The composition of the latter rhenium sulfide solid was found to be $ReS_{2.1}C_{5.5}N_{0.7}H_{5.8}O_{2.0}$. The difference between this solution thermal conversion of $Re(abt)_3$ and the solid-state TGA data allowed us to believe that the former process involved a reduction of the high oxidation state of rhenium to the lower one with 1,2,3,4-tetrahydroquinoline. This reaction also transformed THQ to quinoline and a trace amount of oligomeric materials. The gradual formation of insoluble quinoline oligomers on the rhenium sulfide surface was clearly observed in the IR spectrum of insoluble catalyst intermediates. It showed a steady growth of two new bands at 746 and 821 cm^{-1} corresponding to the C–H out-of-plane deformation of quinoline moiety of oligomer. That gave an important indication of the progression of THQ oligomerization on the surface of rhenium sulfides.

Interestingly, we observed a systematic enhancement of dehydrogenative activity of rhenium sulfide solids as thermal conversion proceeded as shown in Figure 7. At temperatures below 150 °C, where there was no thermal decomposition of $Re(abt)_3$, the quinoline to THQ ratio of 0.46 can be essentially correlated to their thermal equilibration at that temperature. This equilibrium ratio increased slightly to 1.0 at 210 °C. Further increase of this ratio within a reaction period of 5 h indicated an onset of dehydrogenative activity of rhenium sulfide intermediates although it remained a small effect below 210 °C. Above 270 °C, a very sharp rise in dehydrogenation reactivity of the catalyst was ob-

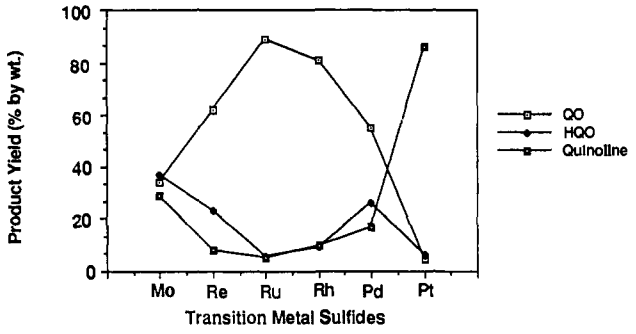

Figure 8. Catalytic dehydrogenative oligomerization reactivity of transition metal sulfides using metal *o*-aminobenzenethiolate complexes as catalyst precursors.

served. It should be noted again that, consistent with all cases, the most reactive rhenium sulfide has a stoichiometric composition approaching ReS_2O_x ($x \approx 2.0$).

To extend the significant results from the $Re(abt)_3$ chemistry, we further investigated the dehydrogenative oligomerization behavior of THQ molecules with other transition metal sulfides using tris- or bis(*o*-aminobenzenethiolate) complexes of groups VIB, VIIB, and VIII transition metals as catalyst precursors. Several metal *o*-aminobenzenethiolate complexes of Ru, Rh, Pt, and Pd were synthesized by a reaction of *o*-aminobenzenethiol with $(NH_4)_2RuCl_6$, $RhCl_3 \cdot 3H_2O$, $H_2PtCl_6 \cdot 6H_2O$, and K_2PdCl_4, respectively.[22] The tris(*o*-aminobenzenethiolato)molybdenum complex $Mo(abt)_3$ was synthesized according to the literature procedure.[7] Elemental analysis of these new *o*-aminobenzenethiol complexes of Ru, Rh, Pt, and Pd fits best with the chemical compositions $Ru(abt)_3$, $Rh(abt)_3$, $Pt(abt)_2$, and $Pd(abt)_2$, respectively. The thermal conversion of these complex precursors to the active CDHP catalyst was carried out in situ in the 1,2,3,4-tetrahydroquinoline solution at 210 °C for 2 h and at 270 °C for 30 min. Under this reaction condition, the final metal and sulfur stoichiometric compositions of the resulting metal sulfides were found to approach MoS_2, ReS_2, RuS, RhS_2, PtS, and PdS, respectively. Further reaction of the same mixture at 270 °C oligomerized THQ molecules to oligoquinolines. Interestingly, we observed a systematic increase in the CDHP activity of these (*o*-aminobenzenethiolate)metal complex derived catalysts from molybdenum sulfide to ruthenium sulfide at a maximum and then decrease to a minimum with platinum sulfide as shown in Figure 8. The change represents a similar periodic trend as that observed for the hydrodesulfurization (HDS) activity of metal sulfides on dibenzothiophene molecules,[2,23] even though the CDHP reaction is a dehydrogenation process and the HDS reaction is a hydrogenation process.

All of the catalysts, which were prepared from their *o*-aminobenzenethiolate complex precursors, used in this study showed a high dehydrogenation reactivity that was demonstrated by a nearly quantitative conversion of 1,2,3,4-tetrahydroquinoline to either oligomeric products or quinoline. The difference in the yield of oligomer products as shown in Figure 8 can be correlated to the relative oligomerization reactivity of the catalyst. A high oligomerization reactivity (95% yield in total) of ruthenium sulfide results in a low yield (5%) of quinoline. In other words, the low oligomerization activity of platinum sulfide is accompanied with a high yield (86%) of quinoline. The degree of polymerization was found to decrease in the order Ru > Rh > Pd > Mo > Re > Pt with the highest yield of chloroform insolubles (the higher molecular weight oligomer) from the reaction using rhenium sulfide as catalyst. From the difference in the yield of HQO, it indicates that the relative dehydrogenation reactivity of these metal sulfides to complete the aromatization of partially hydrogenated quinoline oligomers to quinoline oligomers follows the order Ru > Rh > Re ≈ Pd > Mo. This result substantiated the high efficiency of ruthenium sulfides on the catalytic hydrogenation–dehydrogenation reversibility. A similar CDHP efficiency was also observed on ruthenium sulfide precursors prepared from the reaction of ammonium hexachlororuthenate (IV) and lithium sulfide in ethanol to give 97% yield of combined oligomeric products.

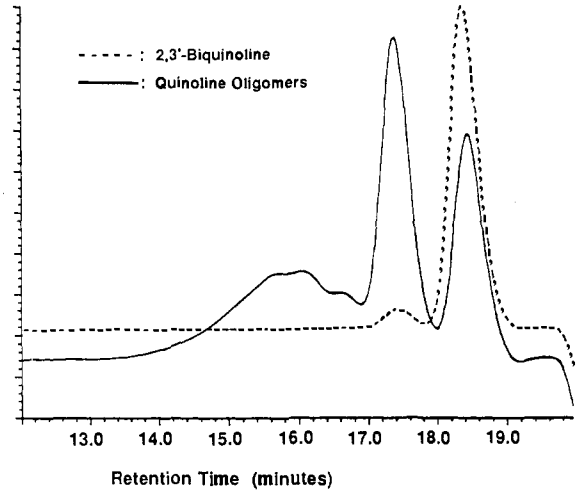

Figure 9. GPC analysis of the diethyl ether insoluble and methylene chloride soluble fraction of quinoline oligomer **1**. The dotted line is the similar GPC run with 2,3'-biquinoline.

The CDHP reaction products in all studies were separated into fractions differing in solubility in solvents of hexane, diethyl ether, methylene chloride, acetic acid, and concentrated HCl. We found that the diethyl ether soluble fraction contained mainly the low molecular weight quinoline oligomers and the partially hydrogenated quinoline oligomers. The fraction of oligomer that is methylene chloride soluble and diethyl ether insoluble contained a small amount of partially hydrogenated quinoline moieties. The amount of aliphatic hydrogen was estimated from the ^1H NMR spectrum to be less than 3%. However, the ^{13}C NMR spectrum of this fraction provided less clear evidence of the existence of aliphatic carbons. In general, partially saturated heterocyclics have a higher polarity than the fully aromatized one. Thus, quinoline oligomers free of aliphatic hydrocarbon can be obtained from this fraction by a filtration through silica gel. The GPC analysis of this fraction (Figure 9) showed the relative intensity of oligomer **1** with $x = 2$ (the first peak), 3 (the second peak), 4 (the third peak), 5 (the fourth peak), and 6–12 (the fifth band). The data were calibrated by a similar run with 2,3'-biquinoline (the dotted line) and styrene oligomers. The methylene chloride insoluble and acetic acid soluble fraction of quinoline oligomers has an estimated average repeating quinoline unit of 11, based on the calculation of the intensity ratio between that of peaks corresponding to the α protons and peaks at 7–8.7 ppm combined in the ^1H NMR spectrum. Finally, the acetic acid insoluble fraction of product, which can be isolated by the extraction with concentrated HCl and subsequently purified from the catalyst residues, presumably have a higher molecular weight than the soluble one.

It is essential to resolve the chemical structure of products in order to understand the origin of the catalytic dehydrogenative polymerization (CDHP) reaction of heterocyclic organic molecules with transition metal sulfides. The structure of quinoline oligomers was elucidated on the basis of the X-ray crystallographic study and various spectroscopic measurements. Elemental analysis led to the formulation of product oligomers as $C_9H_{5+x}N$ close to the expected polyquinoline composition. Presumably, the value of x varies as a function of both the degree of aromatization and oligomerization with a hydrogen atom as an end group. The mass spectrum (electron impact) of the tetrameric quinoline detected in the methylene chloride soluble fraction showed a clear consecutive weight loss of 127, which matches with the m/z value of the quinoline unit in the oligomer. It also showed ion fragmentations of 128, 255, 383, 510, etc., corresponding to the monomeric, dimeric, trimeric, and tetrameric quinoline fragments.

(22) Chiang, L. Y.; Coyle, C. L.; Chianelli, R. R. *Catal. Lett.* **1991**, *8*, 125.
(23) Sinfelt, J. H. *Progr. Solid State Chem.* **1975**, *10*, 55.

Infrared spectrum of quinoline oligomer, compared with that of 1,2,3,4-tetrahydroquinoline itself, showed a new band of 821 cm^{-1}, corresponding to the C–H out-of-plane deformation of heterocyclic ring moiety of quinoline, in addition to a band at 746 cm^{-1} of the C–H out-of-plane deformation of benzene ring moiety of quinoline. This, along with the disappearance of a N–H band and a band at 2800–2930 cm^{-1} corresponding to the aliphatic C–H stretches in the IR spectrum of oligomer, indicated that the heterocyclic ring moiety of oligomer has been fully dehydrogenated.

The acquisition of structural information of the high molecular weight oligomers is limited by their solubility and, therefore, relies mainly on the solid-state ^{13}C NMR measurements. Thus, the actual structural studies of oligomers were performed primarily on the soluble fraction of product. To assure a direct determination on the chemical structure of oligomers, we successfully isolated dimeric quinolines from the hexane-soluble fraction of products by a repeated thin-layer chromatography. Quinoline dimers **2** and **3** were collected roughly in 2 to 1 ratio. Crystals of these two dimers were grown from hexane or ethanol. The crystallographic data reduction and the full structural refinement confirmed **2** and **3** as 2,3′-biquinoline and 2,6′-biquinoline, respectively. The new structure of 2,3′-biquinoline is, in fact, unexpected. The crystal quality of 2,6′-biquinoline is excellent, giving an unweighted residual of only 3.6%. Even though the crystal quality of 2,3′-biquinoline is marginally acceptable, giving an unweighted residual of 9.9%, we experienced no difficulty in locating all the carbon and nitrogen atoms in the structure.

For additional confirmation of these compositions, we studied the 2D COSY ^1H NMR spectra and ^{13}C NMR APT spectra of 2,3′-biquinoline and 2,6′-biquinoline to further verify their structure and also to correlate their spectra to those of oligomers. Complete assignments of protons were made on the basis of the 2D COSY experiment and the proton coupling constants. As shown in Figure 2a,b, we found that the α proton $H_{2'}$ of 2,3′-biquinoline and 2,6′-biquinoline has a most downfield chemical shift of 9.77 and 8.96 ppm, respectively. The latter chemical shift bears close resemblance to that of the α proton of quinoline (8.84 ppm). The further down shift of the H_2 proton of 2,3′-biquinoline is reasoned by a quinoline substitution on the adjacent carbon $C_{3'}$. These chemical shifts are in good agreement with the chemical shift of two groups of peaks in the ^1H NMR spectrum (Figure 2c) of the methylene chloride insoluble and acetic acid soluble fraction of oligomeric products, centered at 9.77 and 8.90–8.95 ppm. They correspond to two kinds of α proton adjacent to the nitrogen atom in the quinoline unit as an end group in a similar structural skeleton to **2** and **3** and one aromatic proton similar to $H_{4'}$ of 2,3′-biquinoline. The third group of peaks centered at 8.60 ppm in Figure 2c was also found to be in a similar chemical shift range of protons $H_{7'}$ and $H_{5'}$ of 2,6′-biquinoline at 8.60 and 8.62 ppm, respectively. Since this methylene chloride insoluble and acetic acid soluble fraction of oligomers contains no dimers, it clearly implies that the structural environment of α protons in oligomers is closely related to that of dimers **2** and **3**. The much lower intensity of these peaks relative to combined intensities of the rest of aromatic protons indicated that one of the ring junctions has to occur at the α carbon next to the nitrogen atom in the oligomer. Utilizing the structure of **2** and **3** as references, we concluded that the primary ring connections between quinoline units in oligomer occur at both C_2–$C_{3'}$ and C_2–$C_{6'}$ carbon positions. The next question then arises as to which of these two ring conjunctions composes the major structure of quinoline oligomer **1**. To resolve this issue, a significant effort was contributed to isolate a limited quantity of a major component of trimer **4** by a repeated analytical GPC fractionation of the methylene chloride soluble fraction of oligomer with a careful collection of materials corresponding to the peak of trimers, followed by thin-layer chromatography for further separation of trimers. The 2D COSY ^1H NMR spectrum of trimer **4** is illustrated in Figure 4. From this 2D experiment and the expanded spectrum, we were able to completely resolve the chemical shift assignment of protons and confirm its structure as consistent with 2,6′:2′,3″-triquinoline. The spectrum shows the most downfield chemical shift of α protons $H_{2''}$ and $H_{4''}$ at

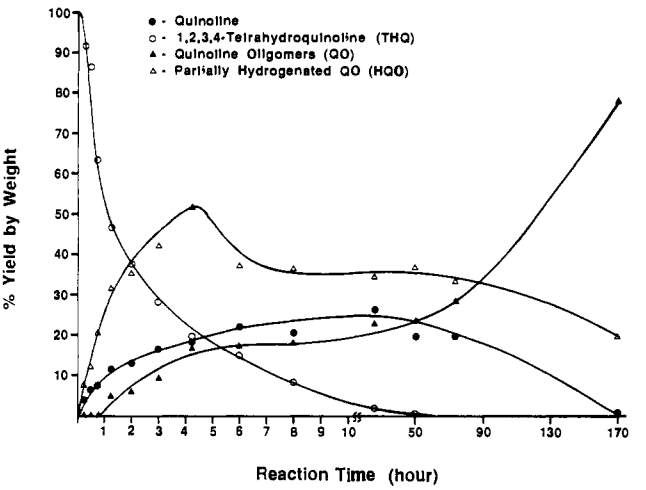

Figure 10. Reaction time dependence of yield (percent by weight) of quinoline, 1,2,3,4-tetrahydroquinoline, partially hydrogenated quinoline oligomer, and quinoline oligomer in the CDHP reaction using a high surface area rhenium sulfide as a catalyst.

9.78 and 9.07 ppm, respectively. The overall chemical shifts of protons in two outer quinoline moieties bear close resemblance to those of corresponding protons in 2,3′-biquinoline. The protons $H_{5'}$ (8.79 ppm) and $H_{7'}$ (8.67 ppm) in the center benzene ring have a nearly 0.9–1.1 ppm shift from that of H_5 and H_7 in the outer benzene ring. All the short- and long-range proton coupling constants can be resolved and assigned as illustrated in Figure 4.

The understanding of the origin of dehydrogenative oligomerization reaction and the elucidation of reaction pathway occurring on the rhenium sulfide surface could be a complex issue. It involves several variable parameters, which influence greatly on the CDHP chemistry, on the catalyst alone, such as crystallinity, surface area, surface structure, chemical composition, and reaction site. At the present stage of study we intended to simplify the surface chemistry and focus on the investigation of molecular transformation of monomer during the CDHP reaction. To follow the conversion of THQ molecules to quinoline oligomers, we carried out the preliminary kinetic measurements of intermediates, such as quinoline, THQ, QO (quinoline oligomers), and HQO (partially hydrogenated quinoline oligomers), in the reaction medium using a high surface area (24–45 m^2/g) rhenium sulfide as a catalyst precursor as shown in Figure 10. The catalyst precursor was thermally activated in situ in the presence of THQ to a hydrocarbon-containing rhenium sulfide with a rhenium vs sulfur composition close to $ReS_{1.9\text{-}2.1}O_x$. The reaction intermediates were sampled and separated by hexane, methylene chloride or chloroform, and methanol into fractions. The hexane-soluble fraction contains predominantly quinoline, THQ, and a small quantity of dihydroquinolines. The relative yield among these intermediates can be monitored by the GC analysis, which was calibrated by quinoline and THQ standards. Both QO and HQO in the hexane-insoluble fraction can be separated from each other by MeOH at 5 °C.

The observation of hydrogen evolution from the reaction solution and a sharp decline of THQ concentration to nearly 50% within 1 h of reaction and to 4% within 10 h of reaction indicated a high dehydrogenation reactivity of the activated rhenium sulfide on THQ molecules. This decrease was accompanied with a sharp increase of HQO to a maximum of roughly 50% yield within 4 h of reaction. It then decreased and reached a steady concentration at 35% yield until the reaction was proceeded for slightly more than 40 h. Interestingly, a significant quantity of quinoline was detected at the early stage of reaction. It increased slowly to 20% yield after 6 h of reaction and then leveled off until roughly 40 h of reaction. The detection of quinoline provides an important insight to the elucidation of the reaction mechanism. Apparently, the formation of quinoline oligomers required an induction period of at least 1 h, followed by a slow increase until 40 h of reaction.

We believe that the initial dehydrogenation of THQ molecules afforded a reactive intermediate of 3,4-dihydroquinoline. This intermediate can be further dehydrogenated to quinoline or isomerized to 1,2-dihydroquinoline and 1,4-dihydroquinoline. However, we are not able to isolate these dihydroquinolines (DHQ) in a significant quantity during the reaction, indicating high reactivity of them under these conditions. Nevertheless, dihydroquinolines can be detected by the GC/mass spectral analysis through the kinetic sampling of reaction intermediates. The relative GC intensity ratios of dihydroquinolines vs quinoline ($I_{DHQ}/I_{quinoline}$) were estimated to be 0.03, 0.05, 0.10, 0.07, 0.06, 0.06, and 0.06 at reaction periods of 15 min, 45 min, 2 h, 4 h, 8 h, 24 h, and 48 h, respectively. The limited fluctuation of this ratio after 4 h of reaction indicated that a steady-state equilibration between DHQ and quinoline as described in the following simplified equation had been reached:

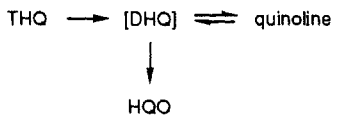

The subsequent thermal oligomerization or condensation reaction between dihydroquinolines gave partially hydrogenated quinoline oligomers (HQO), which are precursors to the product of quinoline oligomers. Therefore, in Figure 10, the decrease of THQ concentration corresponds to an increase of the concentration of both HQO and quinoline. The thermal equilibration between quinoline and THQ in the bulk phase at 270 °C in the presence of the dissolved hydrogen, which is the byproduct of reaction, was not significant enough to maintain a detectable quantity of THQ after 50 h of reaction. However, a slow surface hydrogenation of quinoline to dihydroquinolines consumed quinoline and thus decreased its concentration to zero after 170 h of reaction. Finally, the dehydrogenation of HQO to the product of quinoline oligomers was apparent a slow process that gave a sharp increase of HQO to a maximum in the first 4 h of reaction. Afterwards, the net of production and consumption of HQO led to a slow decrease of its concentration. In principle, if the reaction is allowed to continue for a sufficient amount of time, the dehydrogenative conversion of HQO to QO can be completed.

The scope of this CDHP reaction was evaluated by carrying out similar reactions with various monomers of THQ analog with rhenium sulfides. As a result, we found that, except THQ and 1,2,3,4-tetrahydroquinoxaline, no oligomers were obtained from the reaction with pyrrolidine, piperidine, tetrahydrothiophene, 1,2,3,4-tetrahydronaphthalene, 1,2,3,4-tetrahydroisoquinoline, and quinoline. It implies that a combination of aromatic hydrocarbons and a nitrocyclic ring with an active α-hydrogen atom is an ideal system for the oligomerization to occur. Since quinoline itself was not oligomerized in the presence of rhenium sulfides, it clearly indicated that a stable aromatic quinoline gives no contribution to the oligomer propagation mechanism. In fact, the formation of quinoline during the reaction may actually prolong the completion of oligomerization. On the basis of the structural determination of product and the kinetic understanding discussed above, we proposed a three-step reaction mechanism for this CDHP reaction involving dehydrogenation, oligomerization, and aromatization reactions in a sequence as shown in Figure 11. When 1,2,3,4-tetrahydroquinoline molecules approach to the catalyst surface, the unpaired electrons and π-electrons readily interact with electron-deficient sites of the catalyst surface. The chemisorption of amino hydrogen from THQ molecules onto the surface gives an intermediate **14**. This surface interaction presumably involves the formation of a nitrogen–rhenium bond.[24] To maximize electronic interactions between the aromatic moiety and the surface, the chemisorbed THQ molecule as intermediate **14** is most likely to tilt toward surface. With this particular molecular orientation, the axial hydrogen of the α-carbon tends to contact directly onto surface, making it accessible for chemisorption. That results in a reactive intermediate of 3,4-dihydroquinoline (**15a**). Structure **15a** can be, in principle, reversibly desorbed into the bulk solution. Under the reaction conditions, the thermal isomerization of 3,4-dihydroquinoline may occur in an equilibrium state with 1,4-dihydroquinoline (**15b**) and 1,2-dihydroquinoline (**15c**) both at the surface and in the bulk phase. From the fact that we experienced difficulties in detecting isomeric dihydroquinolines in an appreciable quantity at the early stage of reaction implied either a high reactivity of them under reaction conditions or a low desorption rate for them to diffuse from surface

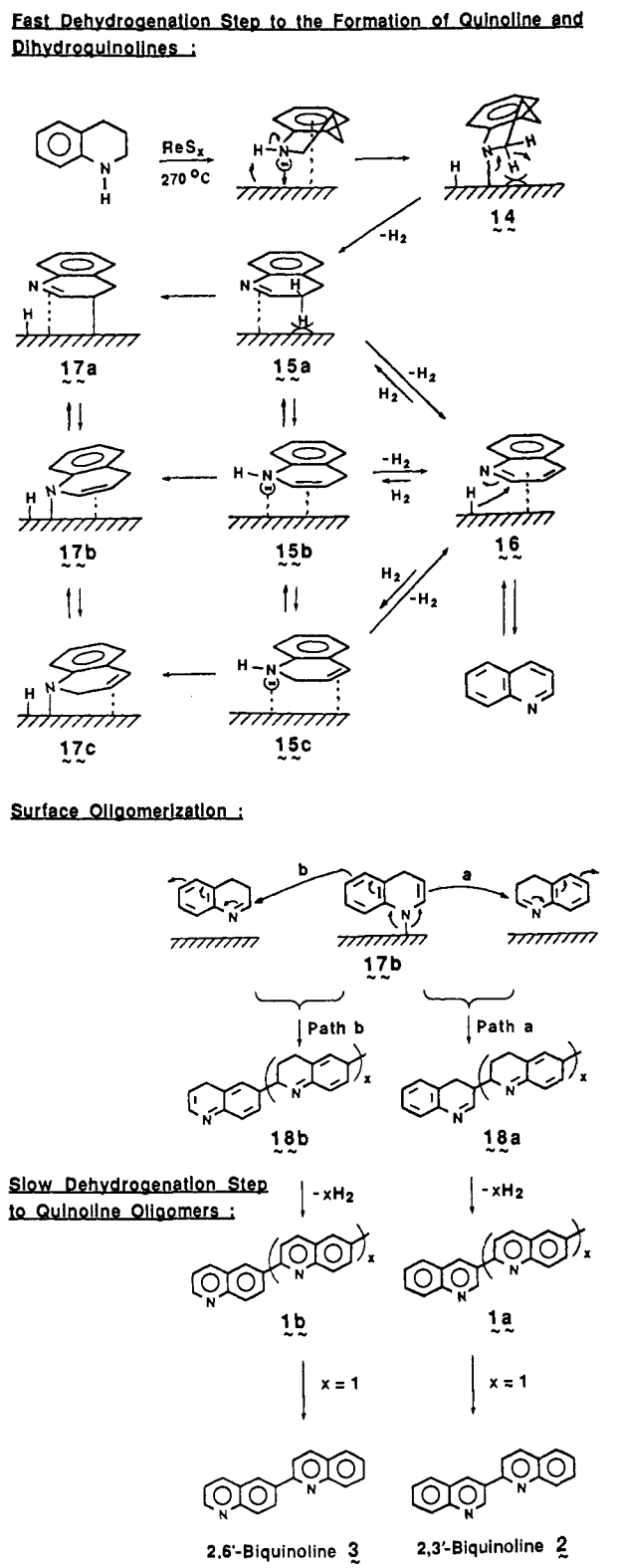

Figure 11. Proposed reaction mechanism of the catalytic dehydrogenative polycondensation (CDHP) reaction of 1,2,3,4-tetrahydroquinoline.

(24) Eisenstadt, A.; Giandomenico, C. M.; Frederick, M. F.; Laine, R. M. *Organometallics* **1985**, *4*. 2033.

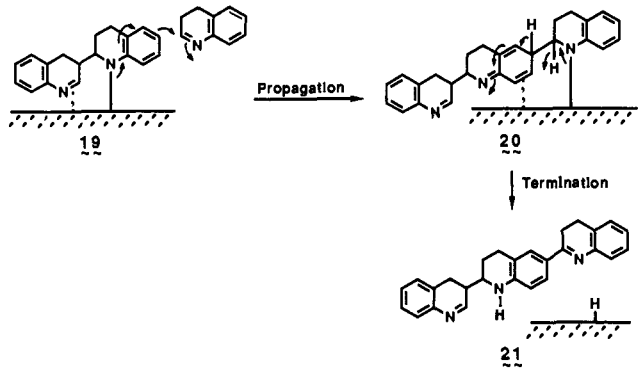

Figure 12. Propagation and termination chemistry of the CDHP reaction.

into solution. In the beginning of the reaction, the catalyst surface is hydrogen deficient. The continuous dehydrogenation of dihydroquinolines to quinoline is favorable until the saturation of hydrogen at the surface is reached. Then, the thermal dehydrogenation–hydrogenation equilibration between dihydroquinoline isomers and quinoline both at the surface and in the bulk phase follows. However, the equilibration is still in favor of the quinoline formation. That results in an excess of hydrogen being evolved from the reaction medium. The chemistry is consistent with the high hydrogen-donating capability of THQ. The sufficient concentration of quinoline at the equilibrium state allows us to monitor the reaction kinetics. Furthermore, after the consumption of DHQ to oligomers becomes significant, a slow reabsorption of quinoline back to the surface followed by the hydrogenation of it to dihydroquinolines completes the cycle of quinoline–dihydroquinolines steady-state equilibration. Further surface dehydrogenation of **15a**, **15b**, and **15c** results in the chemisorbed dihydroquinoline intermediates **17a**, **17b**, and **17c**, respectively. The subsequent thermal oligomerization reaction between 3,4-dihydroquinolines is initiated by the surface-absorbed dihydroquinolines, especially 1,4-dihydroquinoline **17b**, to afford partially hydrogenated quinoline oligomers (HQO). The condensation reaction can undergo the path a or b with the path a as a major route, since path b involves an unfavorable disruption of the benzene aromaticity in **17b**. In the propagation step, the steric hindrance prohibits the 1,2-condensation and favors the 2,6-condensation of 3,4-dihydroquinoline to give HQO **18a** and **18b**. An early termination of chain propagation via dehydrogenation can lead to low molecular weight materials. The further dehydrogenation of HQO to the product of quinoline oligomers **1a** and **1b** was apparently a slow process that required at least 15 h of reaction to effect aromatization. This final step of reaction also serves as the termination of oligomerization. Experimentally, the efficiency of the last two steps of the reaction was found to be dependent on the catalyst concentration. Finally, it is plausible that the thermal condensation between dihydroquinolines in the bulk phase proceeded only in a limited manner and gave lower molecular weight oligomers than those obtained from the surface reaction.

Conclusion

A new catalytic dehydrogenative polycondensation (CDHP) of 1,2,3,4-tetrahydroquinoline (THQ) using transition metal sulfides or tris- or bis(*o*-aminobenzenethiolate) complexes of groups VIB, VIIB, and VIII transition metals as catalyst precursors is described. The method provides a direct route to the synthesis of nonsubstituted quinoline oligomers, which have not been prepared by known methods. The effective heterogeneous CDHP catalysts were generated in situ in reaction media from precursors by a preheating treatment at 180–210 °C. These active catalysts were found to consist of metal and sulfur stoichiometric compositions approaching MoS_2, ReS_2, RuS, RhS_2, PtS, and PdS. We observed a periodic trend on the CDHP activities of transition metal sulfides, showing a maximum oligomer yield (97%) with a ruthenium sulfide catalyst.

The structure of quinoline oligomers was elucidated on the basis of X-ray crystallographic studies and various spectroscopic data including the 2D COSY ^{1}H NMR spectra. The full structural characterization of two quinoline dimers and a trimer, which were successfully isolated from the bulk product, resolved the puzzle of carbon positions at the ring junction between quinoline moieties in compound **1**. A hypothetical CDHP reaction mechanism was proposed that results in two major products of quinoline oligomers **1a** and **1b**, differing only in the orientation of the head unit in structure. We conclude that a delicate balance between dehydrogenation and polymerization activity of catalyst is required to optimize the yield and the molecular weight of resulting products in the CDHP reaction. We also observed the coexistence of hydrogenation and dehydrogenation activity probably at different surface sites of transition metal sulfide.

In the propagation step from **17b** to **19** and then **20** as shown in Figure 12, the growth of oligomer is accomplished by transferring the nitrogen–rhenium bond to the incoming 3,4-dihydroquinoline molecule and proceeds accordingly. The propagation reaction can be terminated whenever the loss of the α-hydrogen adjacent to the bonding site of oligomer on the catalyst surface occurs as depicted in structure **20**. That results in the desorption of partially hydrogenated quinoline oligomers into the bulk phase and a hydrogen-enriched surface **21**. Therefore, in principle, the termination of oligomerization could be suppressed by a treatment of hydrogen enrichment on the surface of catalyst at a proper stage during the reaction. A saturation of hydrogen on the surface will certainly inhibit the dehydrogenation of the α-hydrogen and allow the propagation reaction to continue. However, our attempts to increase the molecular weights of products by either maintaining the reaction media under positive hydrogen pressure or removing hydrogen from the reaction had not led to promising results. More studies on ways to control the hydrogen density on surface throughout the reaction are obviously necessary.

Acknowledgment. We thank R. Chianelli and E. Stiefel of Exxon Research and Engineering Co. and M. Boudart of Stanford University for the discussion of catalysis chemistry related to this work.

Registry No. 2, 612-81-7; **3**, 21132-74-1; THQ (homopolymer), 30496-32-3; THQ, 635-46-1; ReS_2, 37299-85-7; RuS, 37245-92-4; RhS_2, 37245-91-3; PdS, 12648-43-0; PtS, 12627-62-2; MoS_2, 85509-87-1.

Supplementary Material Available: Tables of distances, angles, positional parameters, displacement parameters, torsion angles, and least-squares planes and EIMS for 2,3′-biquinoline and 2,6′-biquinoline (20 pages); listings of observed and calculated structure factors (9 pages). Ordering information is given on any current masthead page.